symmetry

MDPI

Article

Modeling of Particle Size Distribution in the Presence of Flocculant

Elmira Fedorova *, Elena Pupysheva and Vladimir Morgunov

Department of Mineral Processing, Automation of Technological Processes and Production, St. Petersburg Mining University of Empress Catherine II, 199106 St. Petersburg, Russia; s215029@stud.spmi.ru (E.P.); s235016@stud.spmi.ru (V.M.)

* Correspondence: fedorova_er@pers.spmi.ru

Abstract: This study presents a mathematical description of the solid fraction aggregation process in the presence of a flocculant and its result. The basis is a population balance equation. The model is realized in Python language. Verification was carried out using red mud from the investigated enterprise; Flomin AL P 99 VHM was used as a flocculant. The mean square deviation for the parameter "mean aggregate diameter" is equal to 19.88 μm. The time required for the model calculation is about 3 min. The time spent on modeling depends on the number of calculation channels. In this study, 40 channels (20 with PSD source data, and 20 with empty values required for the calculation) were used for the calculation. The time spent on the model calculation is much shorter than the inertia via each of the communication channels for the studied symmetric radial type thickener. A user interface is developed, where the input parameters are the initial pulp particle size distribution, viscosity and density of pulp in the thickener, particle surface area, concentration and flow rate of flocculant, concentration of solid particles, inner diameter and height of the feed well, and simulation time. The result of the simulation is particle size distribution in the feed well of the washer and the mean flocculus diameter.

Keywords: particle size distribution; solid–liquid separation; aggregation algorithm; thickener/clarifier

Citation: Fedorova, E.; Pupysheva, E.; Morgunov, V. Modeling of Particle Size Distribution in the Presence of Flocculant. *Symmetry* **2024**, *16*, 114. https://doi.org/10.3390/sym16010114

Academic Editors: Iver H. Brevik and Vasilis K. Oikonomou

Received: 28 November 2023
Revised: 29 December 2023
Accepted: 10 January 2024
Published: 18 January 2024

1. Introduction

In the examined plant employing the Bayer and Bayer-sintering schemes, the thickening and washing processes play a crucial role in separating red mud from the liquid phase of dilute pulp prior to controlled filtration. This step is essential for minimizing the alkali losses and achieving the final desiliconization of the aluminate solution [1–3]. Enhancing the automated control system, whether through the integration of new control loops or the implementation of an expert control system based on generalized models of a radial thickener, holds the potential to reduce the L:S ratio of the sands by 0.1 unit. This reduction, in turn, corresponds to a 0.25% decrease in alkali losses, leading to a lowered burden on the filters by diminishing the concentration of solids in the discharge from the thickeners [4]. Moreover, this improvement contributes to the stabilization of zones within the thickener, ultimately fostering an increase in the productivity of the operational site.

The radial thickener is a symmetrical cylindrical conical vat with a diameter of 15 m, a settling area of 177 m^2, and an angle of inclination of the cone part of 8°, from which it is clear that the object is characterized by a high level of inertia and lag in most control channels. The washer as a control object is also characterized by a high correlation between the input and output parameters, which makes it difficult to control under constantly acting perturbations, such as: the sludge flow rate in the thickener feed, its particle size distribution, the chemical composition, and the diameter and shape of the flocculated particles [5,6].

The primary purpose of the current automated control systems for the thickening process is to maintain stability in the parameters of the primary technological circuits of

the thickener, treating it as an independent control entity [7,8]. Describing the thickening process as a system characterized by a set of interconnected input and output parameters, it exhibits non-linear relationships. Additionally, various constraints on the control actions exist within this system [9].

To ensure the stable operation of a symmetric thickening apparatus, specific fundamental parameters must be addressed. These include the bed mass, influencing the thickened product's density; the bed level, influenced by the degree of flocculation (refer to the works [10,11] by the researcher Burger, R.A. for further details); and the solid phase content in the upper drain of the symmetric thickening apparatus. In the dynamic conditions of operational production, factors, such as the changes in total pulp flow, variations in leached bauxite composition, disruptions in the leaching process, and manual control, make the thickening process inherently unstable [12–14].

A relevant direction at the moment is the synthesis of models of control objects in order to create software simulators, expert systems, and predictive models on the basis of these models for implementation in the classical structure of automated control systems.

The diagram showing the relationship between various input and output parameters of the thickener/washer is presented in Figure 1. The input process parameters are the feed flow rate, ratio of the flocculant to the solids in the feed, primary particle size, feed solid concentration, flocculation residence time, rake speed, and underflow rate. The output parameters are the overflow solids concentration, bed level, and underflow solids concentration. It is important to note that the input parameters do not affect the final result of the process directly because the process of liquid–solid separation consists of several sub-processes, namely a flocculation sub-model, free sedimentation sub-model, and compaction sub-model.

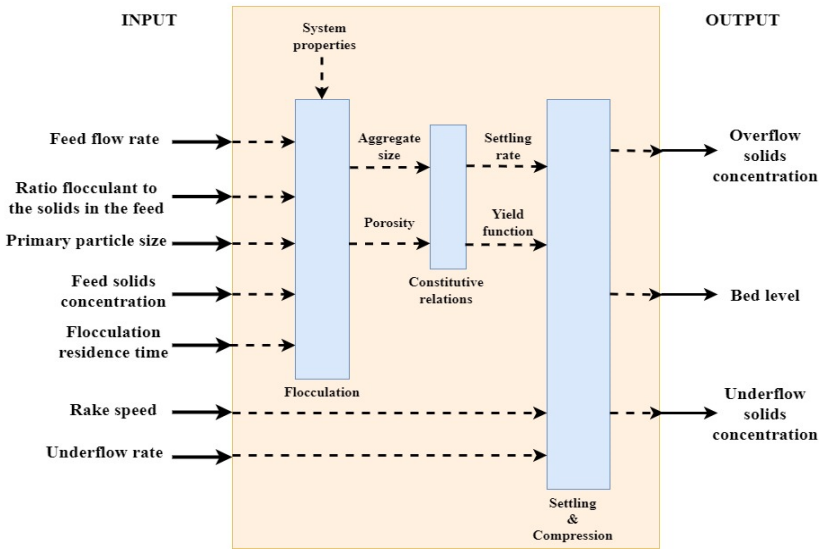

Figure 1. A simplified input–output thickening process diagram. Original images.

In the settling and compression sedimentation zone sub-model, the average size of the flocculated particle obtained from the results of the flocculation sub-model is used as the input parameter [15]. Thus, the population balance model described in this paper is not a stand-alone solution of a separate problem in the framework of the theory of solid particle sedimentation, but only one of the steps for the transition to the description of a complete generalized model of the process occurring in the volume of the apparatus of a single-chamber thickener.

At the moment, there is no information about the complete models describing the all processes in a radial thickener in the open sources. Most often, other researchers describe 1D and 2D models, which do not take into account the clarified zone with the partial removal of solid particles. In the actual systems, the particles within the freely mixed

region can ascend beyond the feed well due to velocity forces, descending into the clarified zone, and subsequently traversing through channels toward the discharge point of the purified aluminate solution. However, the existing models operate under the assumption that the solid fraction from the upper region remains unaffected, and the model addresses the thickener in both the free and constrained sedimentation zones [16,17]. The zone of the rake arm operation is most often omitted in model development. It should be noted that in apparatuses with an implicit conical part, the control of the rake arms' height does not significantly affect the quality of pulp from under the cone of the radial thickener/washer.

This material is the first part of the presentation of the results of scientific research on the development of a generalized model of a single-chamber thickener/washer.

2. Materials and Methods

2.1. Formation of Initial Allocation for PB

A population balance model requires an initial raw material particle size distribution as a starting point for modeling. However, in most cases, the experimental particle size distribution cannot be used directly because the population balance has its own defined channel spacing. This spacing is coarser (fewer channels) than what is specified by most current particle-sizing instruments, in which case the initial population balance size distribution can be obtained by interpolation. The algorithm currently uses linear interpolation. If the experimental size distribution contains only a few data points (e.g., sieve analysis data) or the distribution is highly noisy, the size distribution can first be fitted to a smoothed distribution. The smoothed distribution is then used to interpolate to the original population balance distribution. A lognormal function is used to fit the distribution, i.e.,

$$P_i = \frac{k}{\ln(var)\sqrt{2\pi}} e^{-\frac{1}{2}\left[\frac{(\ln(x_i)-\ln(\overline{x}))}{\ln(var)}\right]^2}, \quad (1)$$

where P_i—percent mass (or volume) of particles in the ith size range; k—constant; var—equivalent of the variance; x_i—mean size of the ith size range; x—volume weighted mean of all the particles.

This is the usual normal distribution, but modified for the logarithmic x-axis. Lognormal distributions are fitted to experimental data using simplex optimization on one of four possible target functions. When fitting to a bell-shaped distribution, the function is of the form:

$$\min_{k,\overline{x},var} \Psi = \sum_i \left(P_i - P_{i,exp}\right)^2, \quad (2)$$

where min Ψ—objective function that needs to be minimized; $P_{i,exp}$—experimental value of P_i.

Particle size distributions typically display significant asymmetry, featuring an elongated tail towards larger sizes on the right side. As a result, they are commonly depicted using a logarithmic x-axis and size intervals that progressively widen in numerical increments. This approach creates a more symmetrical appearance to the distribution, often fitting into a lognormal distribution pattern. Moreover, these distributions can be represented by the number of particles or even the surface area on the y-axis. However, it is more common to plot the percentage by mass (or volume) within each size range. This method accommodates situations where a majority of the sample's mass is comprised of only a few large particles.

If a cumulative distribution is chosen, the target function is of the form:

$$\min_{k,\overline{x},var} \Psi = \sum_i \left(\gamma_i - \gamma_{i,exp}\right)^2, \quad (3)$$

where γ_i—cumulative percent by size i.

This formulation more often weights the objective function toward larger-sized channels compared to a bell-shaped distribution.

Particle size distributions are visualized either as cumulative distributions or in the form of bell-shaped distributions. In the case of a bell-shaped distribution, the *x*-axis represents the particle size, while the *y*-axis represents the number, mass fraction, or percentage of particles within each size range. Although resembling a histogram (vertical bar chart), a dot is commonly positioned at the midpoint of each size channel, and these dots are amalgamated to create a smooth, bell-shaped distribution. This graphical representation enhances the clarity of the particle distribution's shape and the proportion of fines, among other factors.

In contrast, a cumulative distribution is graphed as the percentage of particles passing relative to the particle size. This method utilizes the top size of each size channel instead of the center size, providing an alternative perspective on the distribution pattern.

Red mud from the Sredne-Timansky bauxite mine, obtained during the production internship at the investigated enterprise, was used as feedstock. The chemical composition of bauxite is characterized by a low sulfur content, an increased iron content, and the presence of rare metals (Table 1).

Table 1. Approximate chemical composition of Timan bauxite.

	%		g/t
Al_2O_3	48.69	Ga	80
SiO_2	8.1	Nb	400
Fe_2O_3	27.87	Se	76
TiO_2	2.73	V	510
CaO	0.36	Cr	220
S	0.02	Ni	57
Msi	6.08		

Using a Microsizer 201C instrument made by VA Instalt, Saint-Peterburg, Russia (ultrasonic method; power: 100 W; measurement time: 30 s; transmission coefficient: 73.8%) the particle distribution in the feed slurry of the washer was obtained (Figure 2, Table 2).

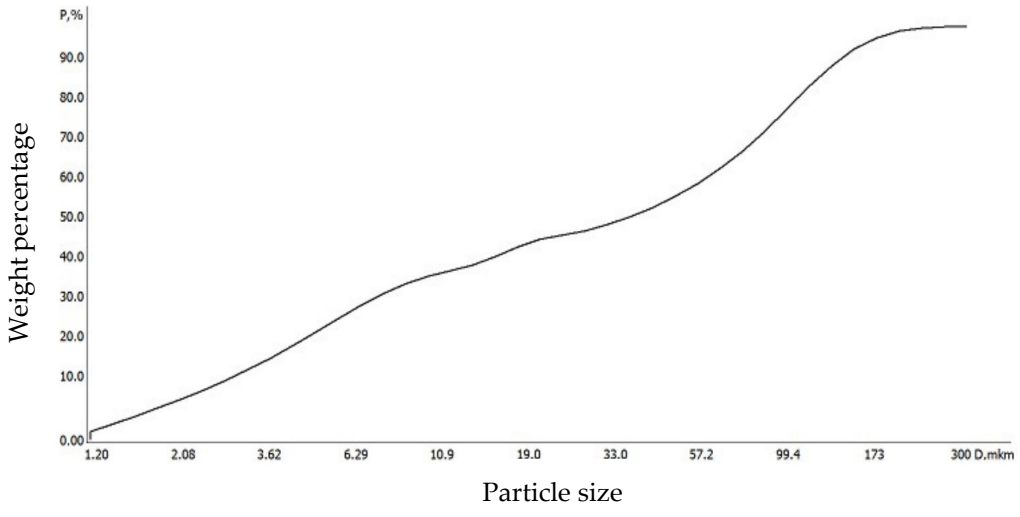

Figure 2. Correspondence of particle sizes (D, μm) to the given values of weight fractions (P, %). Original images.

Table 2. Correspondence of particle sizes (D, μm) to the given values of weight fractions (P, %).

P, %	10	20	30	40	50	60	70	80	90	100
D, μm	2.46	4.24	6.57	11.6	27.4	52.9	76.3	99.5	129	300

The studied pulp sample particle size distribution was in the range of 1.2–300 microns. Based on particle size distribution analysis, it was found that the predominant composition of the solid component consists of smaller classes, with the class below 100 μm constituting approximately 80%.

Consequently, the majority of the sludge comprises particles measuring 100 μm in size. Due to the minimal weight and size of these sludge particles, they exhibit slow settling under gravity. Additionally, given their polydispersity, these particles settle at varying rates, with the larger ones descending more rapidly and frequently colliding with the smaller particles. The presence of larger particles in the sludge contributes to an improved settling effect, resulting in a higher settling velocity for the sludge [18].

It is necessary to take into account the fact that particle size distribution analysis displays only the predominant size of aggregates because the size of suspended particles of red mud is influenced by both natural and anthropogenic factors, such as the chemical and mineralogical composition of the initial bauxite, sample transportation and storage conditions, the amount of time between sampling for analysis and the process of analysis, and chemical dispersion of bauxite particles in the autoclave leaching process.

One way or another, we come to the conclusion that particle size distribution is the most significant property describing the aggregation process in the feed beaker and the sedimentation process as a whole. At the moment, the particle size, in particular, the diameter of floccula from under the feed well, is not measured in real time due to the impossibility of introducing the measuring device into the internal volume of the apparatus. At the investigated plant, the thickeners and washers are under covers; it is practically impossible to install a sensor with periodic introductions into the measured medium to clean the overgrowth on the surface of the slurryAt the investigated plant, the thickeners and washers are under covers; it is practically impossible to install a sensor with periodic introductions into the measured medium and to clean the sensor's surface from overgrowth of the slurry [19,20].

As an intermediate result, the obtained particle size distribution was reduced according to the formulas above to 20 initial channels, which is an input parameter for the population balance model.

2.2. Population Balance Model

The population balance equation (PBE) stands out as a widely employed method for modeling particle aggregation, coagulation, and flocculation. Both foreign and Russian researchers utilize the PBE to model the particle aggregation induced by coagulants, aiming to optimize the subsequent flocculation process [21–23]. Serving as a transfer equation for the particle number density function, the PBE accounts for particle number density functions that vary with time, spatial location, and internal coordinates. These internal coordinates may encompass parameters, such as the volume, surface area, or chemical composition. The dynamics of particle flocculation (aggregation) and the ensuing deflocculation (disintegration) of floccula are captured through particle size distribution (PSD), where the growth and disintegration of floccula populations are expressed as a system of differential equations [24].

The initial stride toward the broader industrial application of PBE models involves crafting a systematic strategy to develop models that are both realistic for industrial plants and mathematically straightforward for online applications [25]. The population balance model is numerically solved as an initial value problem unfolding over time. The simulation commences with the particle size distribution of the feedstock, incorporating additional channels of larger size (empty values) above the initial distribution. Throughout the flocculation process, the particles migrate upward into these channels [26].

Each size channel is characterized by an Ordinary Differential Equation (ODE). Initially, each channel contains a certain number of particles (or none), determined by the initial distribution. Following the addition of a flocculant, the particles start aggregating into larger structures, leading to the disappearance of particles from smaller-sized channels

and their reappearance as aggregates in larger-sized channels. The rate of particle loss or recruitment from each channel is dictated by the aggregation and destruction kernels, with the kernel essentially representing a size-dependent rate equation. Numerical simulation involves small time steps, tracking the particle count in each channel as the model progresses through time [27,28].

A population balance model is a dynamic particle counting system. The population balance approach was first described by Smoluchowski (1917) [29]:

$$\frac{dN_k}{dt} = \frac{1}{2}\sum_{i=1,i+j=k}^{k-1} \beta_{ij} N_i N_j - \sum_{i=1}^{\infty} \beta_{ik} N_i N_k \tag{4}$$

The first term on the right describes the influx of particles into a channel of size k due to aggregation of particles from a smaller size range. Half of the channels are included to avoid the double counting of particles of the smaller sizes i and j. The second term on the right describes the loss of particles of size k as they aggregate with the other particles and migrate upward into larger channels.

Since aggregates can also break up, two additional terms must be introduced to account for loss and gain due to breakup. The second term on the right-hand side of Equation (5) describes the rate of loss of particles of size k due to a fracture, and the last term describes the gain due to fracture of larger aggregates, some of which will yield daughter fragments falling within the size range k [30].

$$\frac{dN_k}{dt} = \frac{1}{2}\sum_{i=1,i+j=k}^{k-1} \alpha\beta_{ij} N_i N_j - \sum_{i=1}^{\infty} \alpha\beta_{ik} N_i N_k - S_k N_k + \sum_{l=k+1}^{\infty} \Gamma_{lk} S_l N_l \tag{5}$$

where N_i—the number of ith sized particles (m^{-3}); t—time (s); α—the capture efficiency [0, 1]; β_{ij}—the rate of collision between i- and j-sized particles (aggregation kernel) (m^3/s); S_k—the breakage rate (kernel) of kth sized particles (s^{-1}); Γ_{lk}—the breakage distribution function (number of k-sized particles produced from the breakage of an l-sized particle).

Equations (4) and (5) are valid only if the channel spacing has a constant width. A typical view of particle size distribution is shown on a logarithmic scale. The logarithmic interval makes the asymmetric distribution of particles more symmetric; this has several additional advantages for modeling population balance. This distribution reduces the total number of equations that need to be solved (which speeds up the modeling process), while maintaining fine resolution on small particles. Different population balance formulas have been proposed using different channel spacings.

The model under study uses the formula of Hounslow (Hounslow, 1988) and Spicer (Spicer, 1996) [31,32]:

$$\begin{aligned}\frac{dN_k}{dt} = &\sum_{j=1}^{i-2} 2^{j-i+1}\beta_{i-1,j}N_{i-1}N_j + \tfrac{1}{2}\beta_{i-1,i-1}N_{i-1}^2 - N_i\sum_{j=1}^{i-1} 2^{j-i}\beta_{i,j}N_j \\ &-N_i\sum_{j=i}^{\infty}\beta_{i,j}N_j - S_iN_i + \sum_{j=i}^{\infty}\Gamma_{i,j}S_jN_j\end{aligned} \tag{6}$$

This population balance formula has a relatively coarse discretization:

$$\frac{V_{i+1}}{V_i} = 2 \; or \; \frac{L_{i+1}}{L_i} = \sqrt[3]{2}, \tag{7}$$

where V_i—the volume of the ith channel; L_i—the length of the ith channel.

The Hounslow model has relatively coarse channel spacing, which allows it to cover the entire size range from the smallest primary particles to the large aggregates in 40 size channels. Despite the coarse channel spacing, the Hounslow model gives accurate results for the zero moment (total number of particles) and the third moment (mass conservation) and only minor errors in the other moments (e.g., the second moment is the surface area).

The size interval is then modified to account for the porosity of the aggregate. Equation (9) is formulated for non-porous particles, i.e., droplet coalescence, and this dimension is retained in the model for particle mass conservation. However, a modified dimension is used to calculate the collision radii, etc.:

$$d_{agg,i} = d_p K_p^{-\frac{1}{3}} \left(\frac{d_{m,i}}{d_p}\right)^{\frac{3}{D_f}}, \quad (8)$$

where $d_{agg,i}$—the diameter of the i-sized aggregate (m); d_p—the diameter of the primary particle (m); $d_{m,i}$—the mass effective diameter of the i-sized aggregate (m); D_f—the fractal dimension (dimensionless); K_p—the particle shape (packing) factor (dimensionless).

Aggregation and Destruction Kernels

The aggregation and fracture kernels describe the physics of the flocculation process and are the most important equations in the model. As noted, they are rate equations describing the rates of aggregation and fracture, but they are called kernels because they are functions of particle size. The aggregation kernel has the form [33]:

$$\beta_{ij} = 1.294 \alpha G \left(a_i + a_j\right)^3, \quad (9)$$

where α—the capture efficiency [0, 1] (taken as M); G—the average turbulent shear rate (s^{-1}); a_i—the radius of the ith particle (m); a_j—the radius of the jth particle (m).

This is the turbulent collision kernel of Saffman and Turner (1956) [34], which is the most widely used and accepted flocculation kernel for fine particles in industrial-scale turbulent flows. Capture efficiency (α) is also included to account for the fact that not all the collisions will be successful.

The fracture kernel is of the form:

$$S_i = \frac{k_2 \varepsilon^{k3} \mu a_{agg,j}}{\theta_f}, \quad (10)$$

where θ_f—effective flocculant surface coverage (kg/m^2); μ—the suspension viscosity (Ns/m^2); ε—the energy dissipation rate per unit mass (m^2/s^3 or J/s k/g); k_2—a model parameter; k_3—a model parameter.

2.3. Auxiliary Equations

In the washer, there are several main and auxiliary points of flocculant dosing: in the feed beaker and in the pipe with the feed slurry before feeding it into the thickener/washer. In this paper, the assumption is made that the aggregations of particles in the beaker and pipe follow the same law. Further, all the modeling constants are obtained in the experiments in the tube.

A number of additional equations are required to input different information into the aggregation and fracture kernels. The capture efficiency (α) in Equation (9) is determined by the mixing index (M):

$$M = 1 - e^{-k_1 \sqrt{f} L/D}, \quad (11)$$

where k_1—the model parameter (dimensionless); L—the length of the pipe since flocculant addition; D—the pipe diameter (m); f—the pipe friction factor (dimensionless).

This equation describes mixing in a turbulent flow in a pipe. Before the addition of the flocculant, the capture efficiency is zero (stable, non-flocculated suspension). After flocculant addition, a complex process of flocculant mixing with the suspension and adsorption of flocculant on the particle surface occurs. As the flocculant adsorbs on the particle surface, the entrapment efficiency increases, and the flocculation process begins. In a population balance model, this complex sequence of steps is summarized and simplistically described by Equation (15).

Since the model is solved in relation to time rather than the pipe length, Equation (11) is translated into the time domain through the average flow velocity in the pipe:

$$M = 1 - e^{-k_1 \Omega}, \tag{12}$$

where for the flow in the pipe, Ω is defined by

$$\frac{d\Omega}{dt} = \frac{\sqrt{f}V}{D}, \tag{13}$$

where V—mean pipe flow velocity (m/s);

i.e., Ω is an additional ode solved by the model.

If either a constant shear rate or a constant energy dissipation rate is chosen, the pipe data are not used, and the equation is reduced to:

$$\frac{d\Omega}{dt} = 1 \tag{14}$$

The fracture kernel (Equation (10)) contains the term θ_f, the effective flocculant surface coverage [30], which is defined as:

$$\theta_f = \frac{m_f}{A_s} M(1 - \Theta) \tag{15}$$

where θ_f—effective flocculant surface coverage (kg/m^2); M—the mixing index given by Equation (11); m_f = the mass of the flocculant (kg); A_s—the surface area of the solid (m^2); Θ—flocculant degradation [0, 1].

Conceptually, it is simply the mass of flocculant per unit particle surface area. The fracture kernel is inversely proportional to the flocculant coverage, i.e., less flocculant gives weaker aggregates, and therefore, increases the fracture rate, resulting in a smaller aggregate size. The dependence of flocculant dosage on surface area means that finer raw material particles with a larger surface area (per unit particle mass) are weaker, and hence, give smaller aggregates, which is consistent with the experimental observations.

The effective coverage also contains a mixing index (M) to account for the fact that the flocculant must adsorb on the surface to have any effect. However, this is mathematically inconvenient because M is zero before the flocculant is added. Consequently, the effective coverage is also zero, and the destruction kernel is either "infinity" or an "error floating divisor of zero". This problem is addressed in two ways. First, the code does not allow M to ever be equal to zero; for this purpose, a minimum small number (1×10^{-10}) is set in the code. This prevents the floating division of zero. Second, the destruction kernel is turned off when the average size of the aggregates approaches the size of the primary particles. This is achieved by multiplying by a smoothed step function:

$$Z = 1 - e^{1 - \frac{\overline{d_{agg}}}{d_p}} \tag{16}$$

This accounts for the fact that the primary particles are not degraded, at least relative to the aggregates and under conditions favorable to flocculation. At the other end of the process, the mild reduction in aggregate size under prolonged shear is modeled using the term Θ, characterizing flocculant degradation. It accounts for the cleavage and/or rearrangement of flocculant chains on the particle surface, resulting in a less effective flocculant that is more prone to aggregate degradation. Flocculant degradation is modeled as an additional differential equation:

$$\frac{d\Theta}{dt} = k_4 \varepsilon^{k_3} \mu \phi_s M \left(1 - \Theta \left(\frac{\phi_{eff}}{\phi_s}\right)^{\frac{1}{3}}\right) \tag{17}$$

Shear Rate and Energy Dissipation: The fluid shear rate (G) and energy dissipation rate (ε) have a significant effect on most aspects of the flocculation process, increasing the rate of agitation, rate of adsorption, rate of aggregation, and breakdown. The shear rate is determined by:

$$G = \sqrt{\frac{\varepsilon \rho_f}{\mu}} \tag{18}$$

where G—the shear rate (s^{-1}); μ—the suspension viscosity (Ns/m^2); ε—the energy dissipation rate per unit mass (m^2/s^3, or J/skg).

For the flow in a pipe, the energy dissipation rate is calculated using the usual pipe friction coefficient equations:

$$\varepsilon = \frac{2fV^3}{D} \tag{19}$$

And for turbulent flow in smooth pipes, the friction coefficient (f) is determined by the Blasius equation:

$$f = \frac{0.0791}{Re^{\frac{1}{4}}} \tag{20}$$

where the pipe Reynolds number is

$$Re = \frac{DV\rho_f}{\mu} \tag{21}$$

And the density of the fluid (suspension and slurry) is calculated from:

$$\rho_f = \rho_s \phi + \rho_l (1 - \phi), \tag{22}$$

where ρ_s—the density of the solid (particles) (kg/m^3); ρ_l—the density of the liquid (kg/m^3); ϕ—the volume fraction of the particles (m^3/m^3—dimensionless).

The viscosity of the suspension increases depending on the volume fraction of the particles. For non-porous particles:

$$\boldsymbol{\mu = \mu_0 \left(1 - \frac{\phi}{\phi_m}\right)^{-k}}, \tag{23}$$

where ϕ_m—the maximum solid fraction, 0.65 (dimensionless); k—2; μ—the suspension viscosity (Ns/m^2); μ_0—the viscosity of the liquid (Ns/m^2).

However, the aggregates are porous, with the porosity increasing with their size relative to the primary particles, so Equation (23) takes the form:

$$\boldsymbol{\mu_s = \mu_0 \left(1 - \frac{\phi}{\phi_m} \left(\frac{\overline{d_{agg}}}{\overline{d_p}}\right)^{3-D_f}\right)^{-k}}, \tag{24}$$

where $\overline{d_{agg}}$—the volume-weighted mean aggregate size (m); $\overline{d_p}$—the volume-weighted mean primary particle size (m).

Typically, in flocculation in pipe flow, an increase in the aggregate size results in an increase in viscosity, which, in turn, decreases the Reynolds number in the pipe, increases the coefficient of friction, and therefore, increases the rate of energy dissipation. Essentially, an increase in the viscosity results in an increase in the pressure drop required to move the slurry through the pipe at a given velocity, so the pump has to work a little harder, and more energy is dissipated in the fluid. As the viscosity increases more than the rate of energy dissipation, the shear rate (Equation (18)) drops.

3. Results

3.1. GUI Development and Model Manipulation

The user interface was built using the Tkinter library, which was installed as a standard Python module. There are four libraries for GUI work in Python: Tkinter; Kivy; Python QT; and wxPython. Tkinter was chosen because the library requires no additional installation and allows you to quickly create applications with a simple GUI. The applications created using this library are cross-platform, i.e., they can run on different operating systems.

The Tkinter module allows you to create applications with a windowed interface containing vector graphics. In particular, the use of the graphical functions of the Canvas widget allows you to build graphs of functions. However, the capabilities of the matplotlib module are much more advanced, and it is desirable to combine the windowed Tkinter applications with the matplotlib graphical functions. This feature is realized with the "composite" canvas FigureCanvasTkAgg, a special class that inherits many of the methods of the Canvas widget and adds the ability to use the graphics functions of the matplotlib module. The FigureCanvasTkAgg class is imported from the matplotlib.backends.backend_tkagg module.

To run the model, it is necessary to enter the known process parameters into the data input windows. Parameters, such as the initial particle size distribution of pulp, viscosity and density of solution, surface area of particles, concentration and flow rate of flocculant, concentration of solid particles, inner diameter of feeding well, and height of feeding cup, are necessary. It is also necessary to specify the modeling time in seconds.

The parameters related to the red mud material and solution properties are constant, as these parameters are related to the mining and geological conditions of the bauxite deposit and process technology, i.e., they are boundary conditions. The surface area parameter is calculated through the initial particle size distribution. The pipe flow rate corresponds to the range of operating characteristic of the pump used in the studied production. The flocculant dosage and feed solid concentration parameters are in the range of process parameters of the enterprise under study (Table 3).

Table 3. Input parameters and their values.

Parameters	Values	Range	Units
Flocculant dosage	0.08	0.05–0.8	kg/t
Feed solid concentration	70	30–150	g/L
Pipe flow rate	40	20–80	L/min
Liquor viscosity	0.001	-	kg/ms
Particle density	3710	-	kg/m^3
Surface area	8.609	-	m^2/mL
Liquor density	1000	-	kg/m^3
Well inner diameter	0.4	-	m
Well height	1	-	m
Simulation run time	30	-	s

To start the solver, it is necessary to click on the button "Start" (Figure 3).

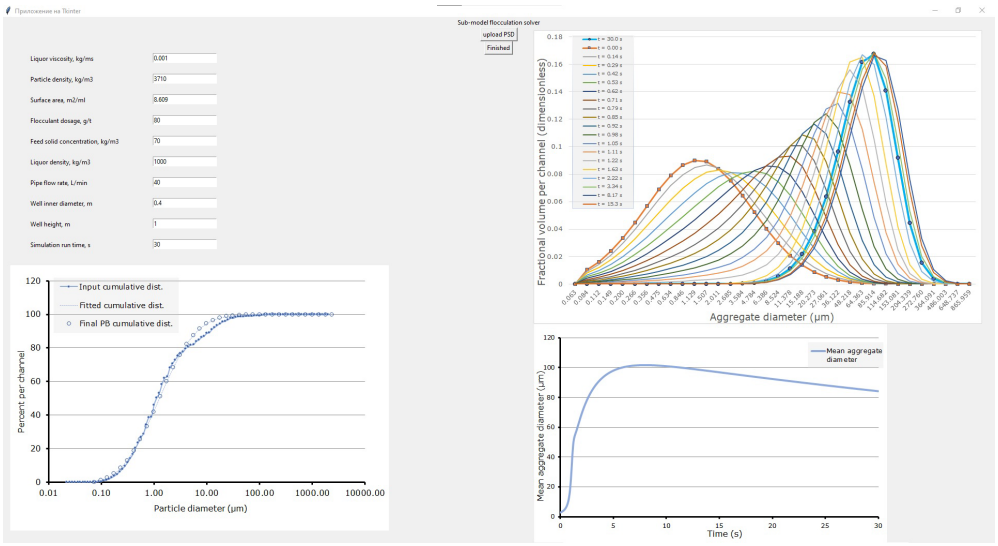

Figure 3. Interface screen for working with the flocculation model. Original images.

The time taken for modeling depends on the initially entered particle size distribution, which depends on the number of calculation channels. The average calculation time of the flocculation model is not more than 3 min.

The model calculates the growth and decay of particles with a certain step and constructs a lognormal particle size distribution (Figure 4). In this study, the slurry predominantly contained fines, which significantly affected the particle distribution of flocculated particles. According to the modeling results, the particulate matter after flocculation is mainly in the following classes 27–153 µm (85.4%). The reason why the distribution becomes narrower in relative terms is that the flocculation process tends to change the aggregates into having an overall stable size. The smaller aggregates combine into larger aggregates, and the larger aggregates are less stable and more likely to be broken up. Flocculus disintegration was also accounted for in the model; the resulting curve is blue with a blue circle mark.

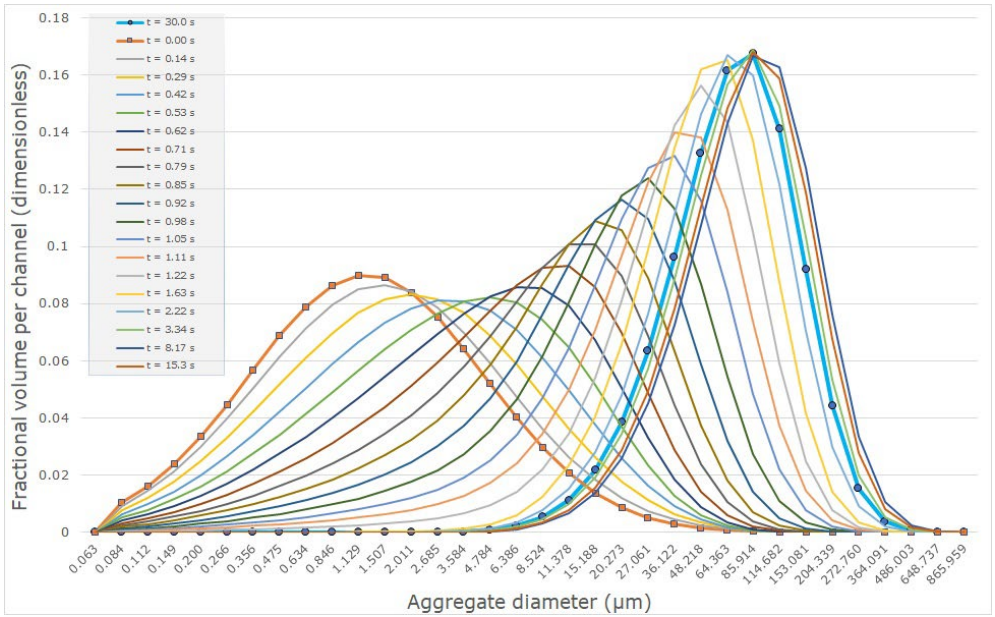

Figure 4. Particle size distribution after the flocculation process (result of the population balance model). Original images.

3.2. Verification of the Algorithm

Since in the described and developed sub-model of flocculation, real initial data were used to verify the result of the algorithm, which were verified using experiments on the sedimentation of pulp in the presence of a flocculant. All the laboratory experiments were carried out with the support of the Scientific Center for Problems of Processing of Mineral and Technogenic Resources of St. Petersburg Mining University of Empress Catherine II and the production laboratory of the investigated enterprise.

For the pulp settling test with the addition of a flocculant, a sample with a solids concentration of 70 g/L was prepared. This value corresponds to the solids content in the feed stream of the thickener/washer.

According to the technology implemented at the studied production facility, the concentration of Flomin AL P 99 VHM flocculant solution fed to the thickener is equal to 0.5%. The aqueous solution of the reagent existed for about 5 days, and it was delivered to the production facility in the form of powder. Such a period is explained by the effect of oxygen on the macromolecule compound; oxygen causes their destruction and reduces the viscosity of the solution used [35].

Immediately before injecting a working solution of flocculant into the cylinder, it was made and left until the emulsion had completely dissolved (the minimum time required is 1.5 h). The technological regulations recommend the use of an additive in the solution in the form of sodium hydroxide in the amount of 10 g per 1 L of flocculant solution, which increases the efficiency of interaction of pulp particles with the flocculant due to the formation of an alkaline environment and leads to a reduction in the amount of polymer used [36,37].

When preparing the flocculant, the following points were taken into account:

(1) The rotation speed of the magnetic stirrer armature during emulsion dissolution should not exceed 2 r/s. This is due to the fact that the rate of sedimentation of flocculates formed during the treatment of the CS reagent at this frequency is several times higher than in the solution prepared at 20 r/s because high speeds of rotation increase the level of tangential stress in the liquid, which leads to the destruction of swollen particles of the flocculant.
(2) The flocculant granules were added directly to the alkaline solution. The solution was stirred for 30 min with a magnetic stirrer, and then it is necessary to leave the prepared solution at rest for 60 min for the formation of macromolecules.

As a result, a flocculant solution with a concentration of 0.5% was obtained.

In the preparation of the slurry under study, it was necessary to measure a 6.9 g suspension of dried sludge from the thickener to dilute with 250 mL of alkaline water (alkali concentration 12 g/L). The slurry was heated in a metal beaker until a temperature between 50 and 80 °C degrees was reached. This temperature range corresponds to the process temperature in the washers. To homogenize the prepared pulp, it was necessary to carry out transfers from beaker to beaker in order to avoid the loss of solid fraction.

A homogenized sample of the prepared slurry with a solid concentration of 70 g/L was placed in a 250 mL measuring cylinder; the initial height before the addition of flocculant was recorded. The dose of flocculant with a concentration of 0.5% was equal to 0.7 mL.

To meet the condition of complete homogenization of the pulp with the preservation of the initial properties of sedimentation, the cylinder was stirred non-intensively ten times by entering the plunger at the height of the beaker; this method of stirring is used in domestic practice in the preparation of the sample for sedimentation [38].

During the sedimentation process, the height of the interface is regularly recorded until a constant height of the thickened product is reached (Figure 5).

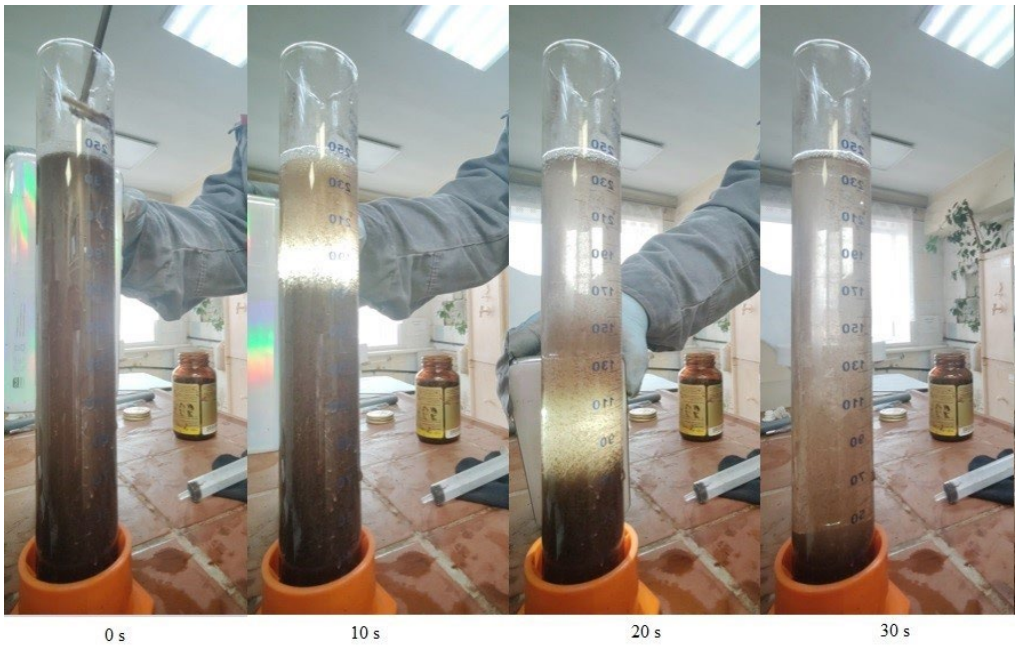

Figure 5. Deposition result of red mud sample with initial concentration of 70 g/L. Original images.

The flocculation time was equal to 30 s; this value was set as a simulation time in the flocculation sub-model (figure with distribution) to match the time of sedimentation of the slurry in the presence of flocculant in the laboratory experiment, since this time was sufficient to carry out complete sedimentation, and thus, complete the flocculation process. During the experimental studies, photographs of clusters of precipitated red mud were obtained, where the floccula (Figure 6) can be characterized as an asymmetric formation surrounding the precipitated aggregates. These images also helped to verify a population balance model that accounts for the size of the deposited aggregates and the symmetry of the floccula. These images were acquired using a microscope and a droplet method of examination. The floccula were sampled using a 2 mL pipette during the interaction process between the precipitated pulp and flocculant and transferred to a microscope slide. An AOMEKIE 64-640 microscope (Ningbo Barride Optics Co., Ltd, Ningbo, China) was used to obtain images of the flocculated pulp.

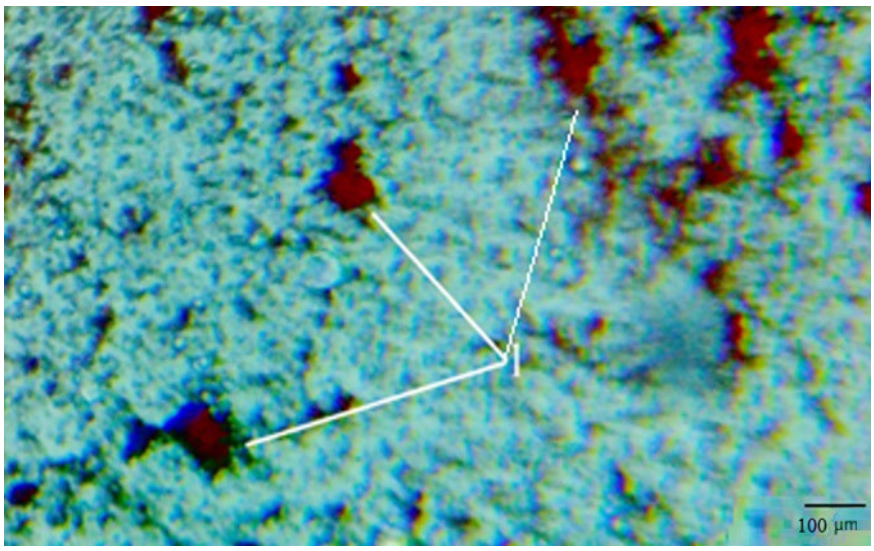

Figure 6. Sample of deposited red mud. Original images.

Since the experiment was carried out in the laboratory of the investigated enterprise, the material parameters of red mud and the properties of the liquor in the laboratory experiment and in the model correspond to the technology. In the laboratory experiment, red mud with a density of 3200 kg/m^3 was used, and the solid concentration corresponds to the process concentration of 70 g/L. The dosage of flocculant injected into a 250 mL cylinder was approximately 0.7–0.9 mL, with a concentration of 0.5%; the error was acceptable due to the equipment used to inject the suspension (syringe). The flocculant dose is directly proportional to the solid content. Since the concentrations of the solid are equal, the volume of flocculant in the laboratory experiment corresponds to the volume of flocculant put in the model.

Thus, the mathematical model and the laboratory experiment have common parameters necessary for the flocculation process. Fifteen red mud settling experiments were conducted in the presence of the flocculant (Table 4). From each cylinder, five samples with floccules were taken. The average particle diameter calculated in the model equal to 84 μm was compared with fifteen different average results obtained in the laboratory experiment. The mean square deviation for the parameter "mean aggregate diameter" was equal to 19.88 μm.

Table 4. Results of the conducted experiment.

Number of Experiments														
1	2	3	4	5	6	7	8	9	10	11	12	13	14	15
Particle diameter in the sample, μm														
143	97	76	138	152	105	127	115	91	120	138	135	89	109	95
92	109	141	112	111	72	111	115	75	45	47	103	152	58	148
38	84	107	119	101	93	69	45	148	92	100	111	101	43	123
131	36	38	70	37	52	130	69	83	38	116	65	114	96	143
63	152	62	131	148	54	98	90	103	113	105	131	62	128	112
Average particle diameter, μm														
93.3	95.7	84.9	113.7	109.9	75.3	107.1	86.8	99.8	81.4	101.3	109.1	103.7	86.8	124.2
Dispersion, μm^2														
395.41														
Mean square deviation, μm														
19.88														

4. Discussion

The red mud-thickening and washing processes are an essential part of alumina production. The site requires the modification of the used processing methods into more technologically advanced and highly efficient ones [39–41].

The size of the floccula and their mean and median diameters directly affect the settling process along the height of the unit in the thickener or washer, the consolidation of the solid phase in the cone bottom of the unit, and the yield of the solid fraction with the top clarified drain of the unit. Sub-processes with particle formation were found, for example, in the following processes: crystallization, agglomeration, grinding, dissolution, leaching, etc.

Since at the investigated enterprise this type of apparatus is used both at the thickening branch and red mud washing branch, it is possible to use the results obtained in the course of the research on the existing structure of ACSPP. For example, these data may be used as an add-on over the existing SCADA system in order to visualize the parameter "mean aggregate diameter of floccula from under the feeding cup" unmeasured in the current conditions on the operator's mnemonic scheme, i.e., a kind of virtual software device for measuring the granulometric composition of the aggregated pulp. Also, this parameter

can be used in the control system as one of the target parameters in the cascade control system to adjust the flocculant flow rate. It should be noted that the process of aggregation occurring in the feeding cup is one of the sub-processes in the thickener or washer of the radial type, and therefore, the model describing the process of flocculation of red mud slurry in the cup is part of the overall model of the control object. Also, this model can be used as a predictive model using advanced process control technology [42,43].

5. Conclusions

This paper presents a detailed mathematical description of the investigated flocculation process and its result after implementation as a model. The model is realized in Python language using a Runge–Kutta solver of the fourth order. The time required to compute the model is about 3 min on an Intel(R) Core(TM) i3-8130U CPU @ 2.20 GHz 2.21 GHz. The mean square deviation for the parameter "mean average flocculus diameter" is equal to 19.88 μm. The time taken to calculate the model is much shorter than the inertia of each of the communication channels for the investigated symmetric radial-type thickener/washer.

A user interface was developed in which the input parameters are the initial pulp size distribution, viscosity and density of the pulp in the thickener, particle surface area, flocculant concentration and flow rate, solids concentration, inner diameter and height of the feed well, and modeling time. The result of the flocculation model, namely the mean aggregate diameter, is used as initial value of the subsequent sub-processes of solid–liquid phase separation.

Author Contributions: Conceptualization, supervision and project administration, E.F.; methodology, formal analysis, software, and writing original draft, E.P.; resources and software, V.M. All authors have read and agreed to the published version of the manuscript.

Funding: This research received no external funding.

Data Availability Statement: Data are contained within the article.

Conflicts of Interest: The authors declare no conflicts of interest.

References

1. Concha, A.F. *Solid–Liquid Separation in the Mining Industry*; Fluid Mechanics and Its Applications; Springer: Cham, Switzerland, 2014; Volume 105, 429p.
2. Kynch, G.J. A theory of sedimentation. *Trans. Faraday Soc.* **1952**, *48*, 166. [CrossRef]
3. Serzhan, S.L.; Skrebnev, V.I.; Malevanny, D.V. Study of the effects of steel and polymer pipe roughness on the pressure loss in tailings slurry hydrotransport. *Ore Process. J.* **2023**, *4*, 41–49. [CrossRef]
4. Zhukovskiy, Y.L.; Korolev, N.A.; Malkova, Y.M. Monitoring of grinding condition in drum mills based on resulting shaft torque. *J. Min. Inst.* **2022**, *256*, 686–700. [CrossRef]
5. Nikolaeva, N.; Aleksandrova, T.; Romashev, A. Effect of grinding on the fractional composition of polymineral laminated bituminous shales. *Miner. Process. Extr. Met. Rev.* **2018**, *39*, 231–234. [CrossRef]
6. Khalifa, A.A.; Bazhin, V.Y.; Ustinova, Y.V.; Shalabi, M.E.K. Study of the kinetics of the process of producing pellets from red mud in a hydrogen flow. *J. Min. Inst.* **2022**, *254*, 261–270. [CrossRef]
7. Koteleva, N.I.; Valnev, V.V.; Korolev, N.A. Augmented reality as a means of metallurgical equipment servicing. *Tsvetnye Met.* **2023**, *4*, 14–23. [CrossRef]
8. Laros, T.; Slottee, S.; Baczek, F. Testing, Sizing, and Specifying Sedimentation Equipment. In *Mineral Processing Plant Design, Practice, and Control: Proceedings Volume 1*; Society for Mining, Metallurgy, and Exploration: Englewood, CO, USA, 2002; Volume 2, 2243p.
9. Fawell, P.; Farrow, J.B.; Heath, A.; Nguyen, T.; Owen, A.T.; Rudman, M.; Scales, P.; Simic, K.; Stephens, D.; Swift, J.D.; et al. 20 years of AMIRA P266 'Improving Thickener Technology'—How has it changed the understanding of thickener performance? In Proceedings of the 12th International Seminar on Paste and Thickened Tailings, Viña del Mar, Chile, 21–24 April 2009. [CrossRef]
10. Bürger, R.; Concha, F. Settling velocities of particulate systems: 12. *Int. J. Miner. Process.* **2001**, *63*, 115–145. [CrossRef]
11. Bürger, R.; Damasceno, J.; Karlsen, K. A mathematical model for batch and continuous thickening of flocculated suspensions in vessels with varying cross-section. *Int. J. Miner. Process.* **2004**, *73*, 183–208. [CrossRef]
12. Salamatov, V.I.; Salamatov, O.V.; Zabolotnyaya, D.Y. To the Issue of Mathematical Modeling of the Red Mud Thickening Process. *Defect Diffus. Forum* **2021**, *410*, 400–404. [CrossRef]

13. Chen, G.; Li, C.; Ruan, Z.; Bürger, R.; Gao, Y.; Hou, H. Structural evolution of bed drainage channels under the shear effect of the whole process of tailings thickening. *Miner. Eng.* **2023**, *203*, 108364. [CrossRef]
14. Ruan, Z.; Wu, A.; Bürger, R.; Betancourt, F.; Wang, Y.; Wang, Y.; Jiao, H.; Wang, S. Effect of interparticle interactions on the yield stress of thickened flocculated copper mineral tailings slurry. *Powder Technol.* **2021**, *392*, 278–285. [CrossRef]
15. Gheshlaghi, M.E.; Goharrizi, A.S.; Shahrivar, A.A. Simulation of a semi-industrial pilot plant thickener using CFD approach. *Int. J. Min. Sci. Technol.* **2013**, *23*, 63–68. [CrossRef]
16. Derlon, N.; Thürlimann, C.; Dürrenmatt, D.; Villez, K. Batch settling curve registration via image data modeling. *Water Res.* **2017**, *114*, 327–337. [CrossRef]
17. Ardila Labiosa, A. Dynamic Simulation of Red Mud Washers Used in Aluminum Industries. Master's Thesis, RMIT University, Melbourne, VIC, Australia, 2010.
18. Madarász, L.; Köte, Á.; Hambalkó, B.; Csorba, K.; Kovács, V.; Lengyel, L.; Marosi, G.; Farkas, A.; Nagy, Z.K.; Domokos, A. In-line particle size measurement based on image analysis in a fully continuous granule manufacturing line for rapid process understanding and development. *Int. J. Pharm.* **2022**, *612*, 121280. [CrossRef] [PubMed]
19. Oksengoyt, E.A.; Kunitskiy, N.A.; Petrov, P.A.; Shestakov, A.K. Modern equipment by Soyuztsvetmetavtomatika for detecting aerosols and spills of harmful pollutants. *Tsvetnye Met.* **2023**, *4*, 61–65. [CrossRef]
20. Golberg, G.Y. Development of the Theory of Formation and Destruction of Flocculation Structures in the Processes of Separation of Suspensions of Fine Coal Enrichment Products. Ph.D. Thesis, Russian Academy of Sciences, Moscow, Russia, 2019; p. 46.
21. Nopens, I.; Biggs, C.; De Clercq, B.; Govoreanu, R.; Wilén, B.-M.; Lant, P.; Vanrolleghem, P. Modelling the activated sludge flocculation process combining laser light diffraction particle sizing and population balance modelling (PBM). *Water Sci. Technol.* **2002**, *45*, 41–49. [CrossRef]
22. Ma, J.; Fu, K.; Fu, X.; Guan, Q.; Ding, L.; Shi, J.; Zhu, G.; Zhang, X.; Zhang, S.; Jiang, L. Flocculation properties and kinetic investigation of polyacrylamide with different cationic monomer content for high turbid water purification. *Sep. Purif. Technol.* **2017**, *182*, 134–143. [CrossRef]
23. Xu, H.; Tian, H.; Deng, J.; Zhuo, Q.; Cui, J.; Wang, J.; Yin, Y.; Yu, P. Review of influence of steric effect on aggregation behavior of fine particles. *Miner. Eng.* **2023**, *203*, 108304. [CrossRef]
24. Quezada, G.R.; Ayala, L.; Leiva, W.H.; Toro, N.; Toledo, P.G.; Robles, P.; Jeldres, R.I. Describing Mining Tailing Flocculation in Seawater by Population Balance Models: Effect of Mixing Intensity. *Metals* **2020**, *10*, 240. [CrossRef]
25. Health, A.R.; Koh, P.T.L. Combined population balance and CFD modeling of particle aggregation by polymeric flocculant. In Proceedings of the Third International Conference on CFD in the Minerals and Process Industries CSIRO, Melbourne, VIC, Australia, 10–12 December 2003.
26. Barthelmes, G.; Pratsinis, S.; Buggisch, H. Particle size distributions and viscosity of suspensions undergoing shear-induced coagulation and fragmentation. *Chem. Eng. Sci.* **2003**, *58*, 2893–2902. [CrossRef]
27. Ahrens, R. Efficient Numerical Treatment of Aggregation Integrals in Multivariate Population Balance Equations. Ph.D. Thesis, Technischen Universität Hamburg, Hamburg, Germany, 2020.
28. Biggs, C.A.; Lant, P.A. Activated sludge flocculation: On-line determination of floc size and the effect of shear. *Water Res.* **2000**, *34*, 2542–2550. [CrossRef]
29. Von Smoluchowski, M. Versuch einer mathematischen Theorie der Koagulations kinetik kolloider Lösungen. *Z. Phys. Chem.* **1917**, *129*, 129–168.
30. Heath, A.R.; Bahri, P.A.; Fawell, P.D.; Farrow, J.B. Polymer flocculation of calcite: Population balance model. *AIChE J.* **2006**, *52*, 1641–1653. [CrossRef]
31. Hounslow, M.J.; Ryall, R.L.; Marshall, V.R. A discretized population balance for nucleation, growth, and aggregation. *AIChE J.* **1988**, *34*, 1821–1832. [CrossRef]
32. Spicer, P.T.; Pratsinis, S.E. Shear-induced flocculation: The evolution of floc structure and the shape of the size distribution at steady state. *Water Res.* **1996**, *30*, 1049–1056. [CrossRef]
33. Veerapaneni, S.; Wiesner, M.R. Hydrodynamics of fractal aggregates with radially varying permeability. *J. Colloid Interface Sci.* **1996**, *177*, 45–57. [CrossRef]
34. Saffman, P.G.; Turner, J.S. On the collision of drops in turbulent clouds. *J. Fluid Mech.* **1956**, *1*, 16–30. [CrossRef]
35. Gandurina, L.V. Organicheskie flokulyanty' v Texnologii Ochistki Prirodny'x i Promy'Shlenny'x Stochny'x vod i Obrabotki Osadka. Inzhenernoe Obespechenie ob"Ektov Stroitel'stva: Obzornaya Informacii/VNIINTPI,-M. 2000, pp. 2–59. Available online: https://meganorm.ru/Data2/1/4293841/4293841858.htm (accessed on 20 October 2023).
36. Salamatov, O.V.; Salamatov, V.I. O vliyanii flokulyantov na kinetiku processov obezvozhivaniya i promy'vki krasny'x shlamov iz nizkokremnisty'x boksitov pri proizvodstve glinozema. *Vestn. Irkutsk. Gos. Texnicheskogo Univ.* **2019**, *23*, 404–414. [CrossRef]
37. Petrakov, D.G.; Loseva, A.V.; Alikhanov, N.T.; Jafarpour, H. Standards for Selection of Surfactant Compositions used in Completion and Stimulation Fluids. *Int. J. Eng.* **2023**, *36*, 1605–1610. [CrossRef]
38. Romashev, A.O.; Nikolaeva, N.V.; Gatiatullin, B.L. Adaptive approach formation using machine vision technology to determine the parameters of enrichment products deposition. *J. Min. Inst.* **2022**, *256*, 677–685. [CrossRef]
39. Piirainen, V.Y.; Barinkova, A.A. Development of composite materials based on red mud. *Obogashchenie Rud* **2023**, *3*, 35–41. [CrossRef]

40. Krizsky, V.N.; Kosarev, O.V.; Alexandrov, P.N.; Luntovskaya, Y.A. Mathematical modeling of the electric field of an in-line diagnostic probe of a cathode-polarized pipeline. *J. Min. Inst.* **2023**, *2023*, 1–10.
41. Ilyushin, Y.V.; Kapostey, E.I. Developing a Comprehensive Mathematical Model for Aluminium Production in a Soderberg Electrolyser. *Energies* **2023**, *16*, 6313. [CrossRef]
42. Dubovikov, O.A.; Beloglazov, I.I.; Alekseev, A.A. Specific features of the use of pulverized coal fuel in combined chemical processing. *Obogashchenie Rud* **2022**, *2022*, 32–38. [CrossRef]
43. Bazhin, V.Y.; Masko, O.N.; Martynov, S.A. Automatic burden balance monitoring and control in the production of metallurgical silicon. *Tsvetnye Met.* **2023**, *4*, 53–60. [CrossRef]